



FBXL20-mediated ubiquitination triggers the proteasomal degradation of 4-1BB

Ruoxuan Sun¹  and Seung-Oe Lim^{1,2,3} 

¹ Department of Medicinal Chemistry and Molecular Pharmacology, Purdue University, West Lafayette, IN, USA

² Purdue Institute of Drug Discovery, Purdue University, West Lafayette, IN, USA

³ Purdue Center for Cancer Research, Purdue University, West Lafayette, IN, USA

Keywords

4-1BB; degradation; FBXL20; ubiquitination

Correspondence

Seung-Oe Lim, Department of Medicinal Chemistry and Molecular Pharmacology, Purdue Institute of Drug Discovery, Purdue Center for Cancer Research Purdue University, West Lafayette, IN 47907, USA
 Tel: +1-765-494-3531
 E-mail: limsoe@purdue.edu

(Received 23 October 2021, revised 27 December 2021, accepted 1 February 2022)

doi:10.1111/febs.16383

4-1BB [tumor necrosis factor receptor superfamily (TNFRSF9), CD137] is a critical immune stimulator that sustains T cell activity and antitumor immune response. The strategy to eliminate cancers by agonistically targeting 4-1BB is under clinical investigation. As a protein expressed in an inducible manner, 4-1BB is under tight control on both transcription and translation levels to maintain its homeostasis. So far, the mechanisms underlying the transcriptional activation of 4-1BB have been well-interpreted; however, it remains inexplicit how 4-1BB is regulated on the protein level. In this study, we presented experimental evidence supporting that 4-1BB, especially the heavily *N*-glycosylated (mature) form, is polyubiquitinated and subjected to the ubiquitin-proteasomal system for degradation. By performing proximity-dependent biotin identification screening coupled with biochemical assays, we identified that F-box/LRR-repeat protein 20 acts as the E3 ligase that promotes the polyubiquitination of 4-1BB at the intracellular domain. Our data provided mechanistic insight into 4-1BB regulation on the protein level by unmasking, for the first time, a posttranslational mechanism governing 4-1BB abundance in cells. The findings of this study could potentially guide the development of 4-1BB-targeted therapy for cancers as well as other immune disorders.

Introduction

The clinical application of immunotherapy has achieved extraordinary success in a broad spectrum of solid and hematopoietic cancers [1]. By blocking the coinhibitory immune checkpoints (e.g., PD-(L)1, CTLA-4) with therapeutic antibodies, the compromised antitumor immunity can be revitalized and, therefore, lead to regression or elimination of the malignancies. However, a large proportion of patients are refractory to checkpoint blockade, and the reasons accounting for it are complicated and still not well-interpreted yet [2]. While the mechanistic investigation regarding immunotherapy resistance remains one of the research hotspots, the

therapeutical potential of novel targets is under intensive exploration to upgrade the cancer immunotherapy arsenal. Among them, the immune-stimulatory receptors such as 4-1BB, OX40, GITR, and CD40 have emerged as attractive targets for drug development [3].

4-1BB (CD137/TNFRSF9), a member of the TNFRSF, was identified as a potent costimulatory receptor on activated T lymphocytes as well as other types of leukocytes [4]. The nuclear factor κ B (NF- κ B) and activating protein-1 (AP-1) serve as key transcription factors driving 4-1BB expression upon immune cell activation [5]. The signal transduction of 4-1BB

Abbreviations

BFA, brefeldin A; BioID, proximity-dependent biotin identification; CHX, cycloheximide; DC, dendritic cell; FBXL20, F-box/LRR-repeat protein 20; PTM, posttranslational modification; TCGA, The Cancer Genome Atlas Program; TNFRSF, tumor necrosis factor receptor superfamily; Ub, ubiquitin; UPS, ubiquitin-proteasome system.

follows a similar pattern shared by TNFRSF family receptors [6]. In general, the trimeric 4-1BB ligand (4-1BBL/TNFSF9) on antigen-presenting cells promotes the clustering of 4-1BB, which afterward recruits the TNFR-associated factor (TRAF) family proteins as key adaptors to transduce signals down to the nucleus [7]. Reinvigorating the antitumor immunity by agonistic anti-4-1BB monoclonal antibodies has demonstrated promising efficacy in many syngeneic animal cancer models [8-10]. Clinically, urelumab and utomilumab as two agonistic antibodies of 4-1BB have entered early-stage trials against solid and hematopoietic tumors. However, limitations regarding the efficacy and liver toxicity became substantial obstructions making them unable to proceed into late-phase clinical studies [11]. Currently, a growing variety of 4-1BB-targeting strategies are being actively investigated in wish to achieve both effectiveness and safety profile. These approaches include combinational therapy [12], Fc-optimized or -deleted 4-1BB antibodies with reduced toxicity [13-17], probodies activated by tumor-associated proteases [18], as well as bispecific antibodies that simultaneously target 4-1BB and other cancer-associated receptors (e.g. PD-L1, HER2) [19,20], etc. A more successful application of 4-1BB is to incorporate the cytoplasmic domain of 4-1BB in chimeric antigen receptors (CARs) for T-cell therapy. As reported, the presence of 4-1BB signaling potentiates the survival and function of CAR-T cells against cancers [21-23].

Despite the mounting research effort focused on the pharmacology and toxicology of 4-1BB therapy, there remains a fundamental knowledge gap to understand how 4-1BB is regulated intracellularly especially on the protein level. There are known to be more than 400 types of posttranslational modification (PTM) that can modulate the properties of proteins, and therefore, give rise to the numerous complexity of proteomes along with the diverse physiological functions [24]. Ubiquitination is a highly conserved PTM that participates in a variety of eukaryotic biological processes, and the most essential one is to maintain proteome homeostasis by initiating the protein degradation process. It was estimated that more than 80% of proteins go through the ubiquitin (Ub)-proteasome system (UPS) for clearance in mammalian systems [25]. In the past years, the growing diversity of nondegradative functions (e.g., protein-protein interaction, signal transduction) of ubiquitination has been unveiled. The cascade reaction of protein ubiquitination is carried out by Ub activation (E1), conjugation (E2), and ligation (E3) enzymes. More than 600 E3 ligases are encoded by the human genome [26], and the majority

of them have a substrate-specific manner of target recognition. Therefore, it is challenging but crucial to identify the enzymes, especially E3 ligases, that ubiquitinate the specific targets of interest. Over the years, significant progress has been made to study the association of protein ubiquitination/deubiquitination in immune responses [27-29]. Dysregulated protein ubiquitination is associated with multiple types of immunological disorders, including inflammation, autoimmune diseases, and cancer. The appreciation of ubiquitination-mediated degradation of significant drug targets may provide considerable opportunities to improve the current therapeutics.

In this work, we elucidated that the cellular abundance and stability of 4-1BB are regulated by ubiquitination on its intracellular domain. F-box/LRR-repeat protein 20 (FBXL20) was identified through proximity-dependent biotin identification (BioID) screening as an E3 ligase catalyzing 4-1BB polyubiquitination and proteasomal degradation. Understanding the molecular basis of 4-1BB turnover could further advance the development and optimization of 4-1BB-targeted therapies in the future.

Result

4-1BB is associated with enhanced antitumor immunity

4-1BB is generally accepted as an immune-stimulatory molecule. To investigate the involvement of 4-1BB in cancer development, we first examined The Cancer Genome Atlas (TCGA) dataset of skin cutaneous melanoma (SKCM) patients and discovered the significantly prolonged overall survival (OS) of individuals whose TNFRSF9 mRNA levels are above average (Fig. 1A). Next, we set out to assess whether 4-1BB contributes to the clinical benefits of immune checkpoint therapy in cancer. As uncovered by the Tumor Immune Dysfunction and Exclusion (TIDE) platform [30], melanoma patients with higher 4-1BB expression are more likely to respond to immune checkpoint therapy (Fig. 1B). We also learned from the Tumor Immune Estimation Resource (TIMER2.0) [31] that the TNFRSF9 mRNA level is associated with augmented tumoral infiltration of CD4⁺ T cells, CD8⁺ T cells, natural killer cells, and antitumor M1 macrophages. On the other hand, 4-1BB is negatively correlated with the abundance of immune-inhibitory cell groups including myeloid-derived suppressive cells (MDSC) and M2-macrophages (Fig. 1C). Together, these findings cooperatively supported that 4-1BB suppresses cancer progression and shapes an inflamed

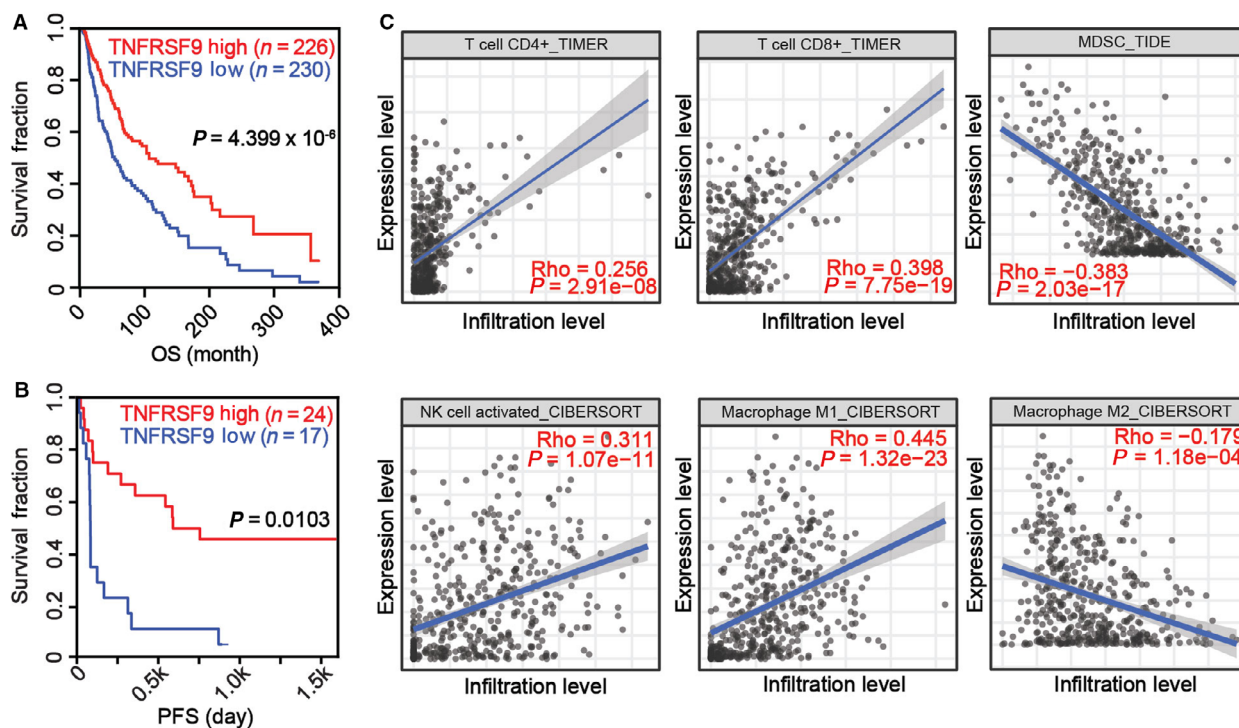


Fig. 1. Prognostic and immune cell infiltration analysis of 4-1BB in cancers. (A) Kaplan–Meier survival analysis of melanoma patients with high ($n = 226$) and low ($n = 230$) *TNFRSF9* expression (TCGA-SKCM dataset). (B) Kaplan–Meier plot demonstrating the correlation of *TNFRSF9* mRNA level and the PFS of melanoma patients undergoing anti-PD-1 therapy (PRJEB23709 dataset, $n = 41$). (C) Impact of *TNFRSF9* on the infiltration of CD4⁺ T cell, CD8⁺ T cell, MDSC, NK cells, M1 macrophages, and M2 macrophages in TCGA-SKCM dataset ($n = 471$). The P values were calculated by log-rank analysis (A–B) and Spearman's correlation analysis (C). OS, overall survival; PFS, progression-free survival.

tumor microenvironment, which is susceptible to immunotherapeutic agents.

4-1BB is a polyubiquitinated protein

Considering the essentiality of 4-1BB in the tumor immune microenvironment, we aimed to study the regulation of 4-1BB with a primary focus on protein level, which has never been reported yet. Protein ubiquitination, one of the most frequently occurred PTMs, is well-characterized as a signal of target degradation through the 26S proteasome. As indicated by the previously published proteome-wide studies, 4-1BB can be ubiquitinated on its intracellular domain [32,33]. Inspired by that information, we conducted immunoprecipitation and mass spectrometry studies to verify the formation of ubiquitination on 4-1BB. As shown in Fig. 2A–B, both human and murine 4-1BB can be polyubiquitinated in cultured cell lines. Liquid chromatography-tandem mass spectrometry (LC-MS/MS) analysis on immunoprecipitated flag-tagged human 4-1BB from HEK293T cells unveiled di-glycine remnant

on K214, K218, K219, and K225 residues with high confidence (Fig. 2C), which provided solid evidence of ubiquitination on these sites (designated as 4-K motif). Sequence analysis indicated that the 4-K motif is highly conserved among mammalian species (Fig. 2D), suggesting potential functions lying within this area.

4-1BB is degraded via UPS

Through biochemical and proteomics study, we managed to identify the ubiquitination sites of human 4-1BB. Next, we aimed to elucidate the biological importance of this modification in detail. As expected, mutation of the four lysine residues results in greatly rendered polyubiquitination of 4-1BB (Fig. 3A). In Fig. 3B–C, we conducted cycloheximide (CHX)-chase assay on HEK293T cells and found that the 4KR mutant (K214/218/219/225R) of 4-1BB exerts markedly augmented stability versus the WT. To characterize whether 4K ubiquitination governs 4-1BB stability in T lymphocytes, we established Jurkat cell lines (4-1BB negative) stably overexpressing the WT or 4KR

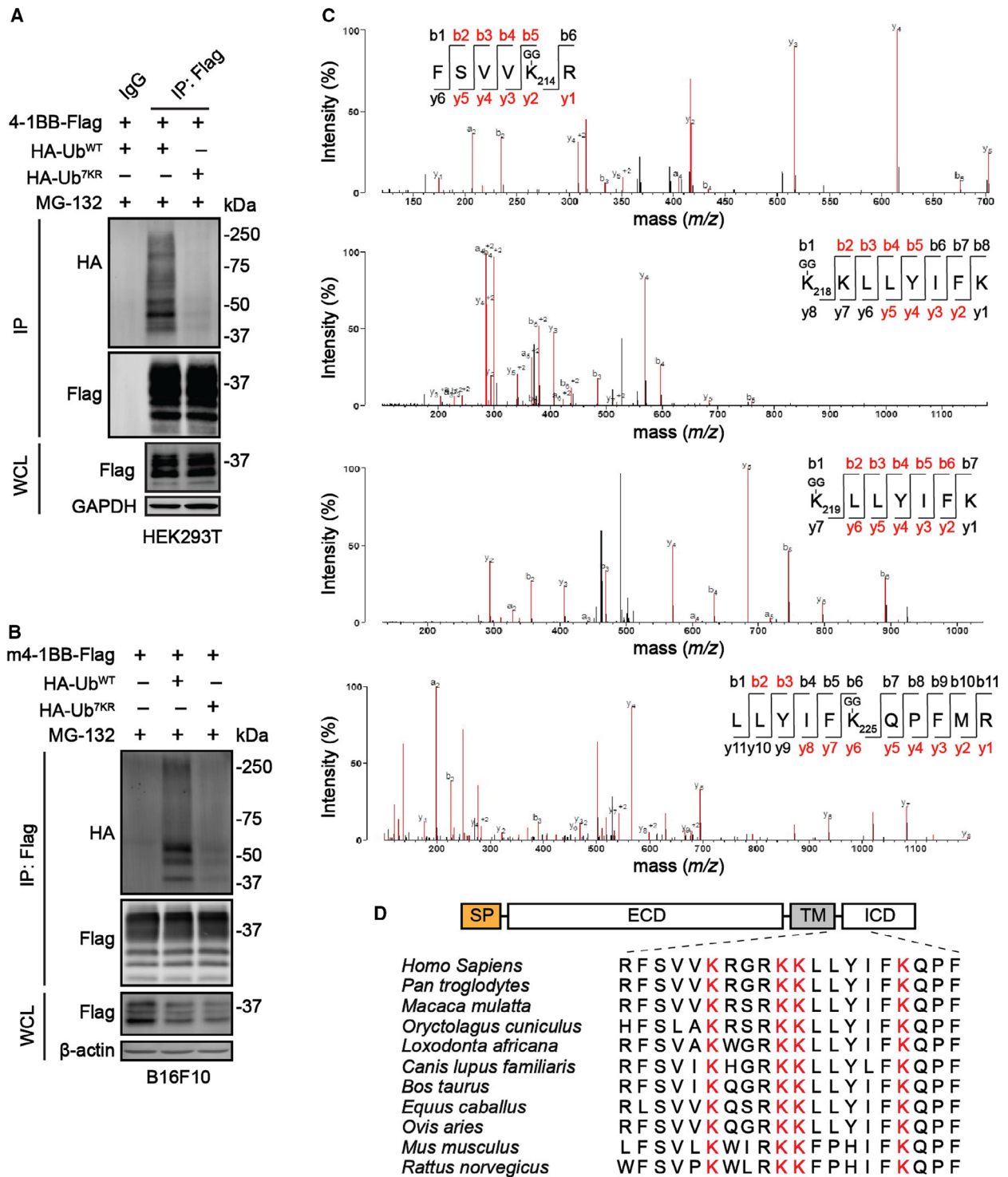


Fig. 2. Validation of 4-1BB ubiquitination in cultured cell lines. (A) Ubiquitination of human 4-1BB was detected in HEK293T cells transfected with 4-1BB-Flag and HA-Ub constructs. The polyubiquitination level of human 4-1BB was detected by *in vivo* ubiquitination assay. (B) Ubiquitination of mouse 4-1BB was detected in B16F10 cells transfected with m4-1BB-Flag and HA-Ub plasmids. The polyubiquitination level of mouse 4-1BB was detected by *in vivo* ubiquitination assay. (C) Tandem mass spectrum of a human 4-1BB fragment with ubiquitinated K214, 218, 219, and 225 residues. The recognized y and b ions were highlighted in red. (D) Amino acid sequence alignment of mammalian 4-1BB on its ubiquitinated region located in the intracellular domain. WCL, whole-cell lysate; IP, immunoprecipitates.

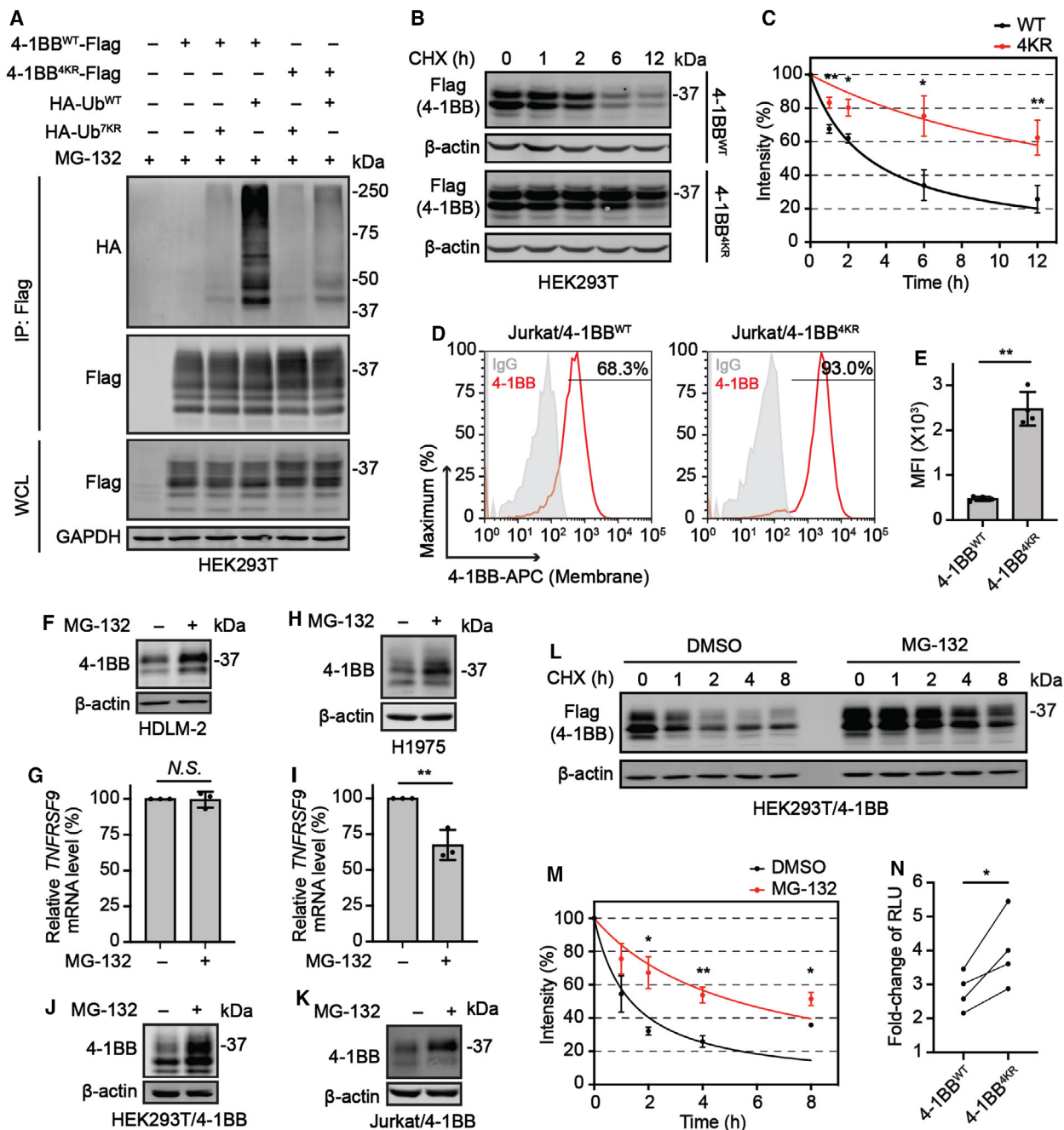


Fig. 3. Turnover of 4-1BB is determined by ubiquitination. (A) *In vivo* ubiquitination assay comparing the ubiquitination of 4-1BB WT and 4KR. The indicated plasmids were cotransfected to HEK293T cells followed by *in vivo* ubiquitination assay. (B) CHX-chase assay comparing the degradation of 4-1BB WT and 4KR. HEK293T cells were transfected with flag-tagged 4-1BB plasmids followed by CHX (100 μ M) treatment for indicated periods of time. (C) Quantification of immunoblotting results in (B) ($n = 3$). (D) Flow cytometry analysis comparing membrane level of 4-1BB WT and 4KR. Jurkat cells were transduced with lentivirus encoding 4-1BB WT or 4KR followed by flow cytometry detection. (E) Quantification of membrane 4-1BB WT and 4KR level in (D) ($n = 4$). (F–I) Proteasome inhibition by MG-132 treatment led to 4-1BB protein accumulation by not mRNA upregulation in HDLM-2 (F, G) and H1975 (H, I). (J, K) Proteasome inhibition by MG-132 treatment led to upregulation of ectopically expressed 4-1BB ectopically in HEK293T (J) and Jurkat cells (K). (L) CHX-chase assay comparing the degradation of 4-1BB with or without proteasome inhibition. HEK293T/4-1BB cells were pretreated with DMSO or 10 μ M MG-132 for 2 h, then incubated with CHX (100 μ M) for indicated periods of time. (M) Quantification of immunoblotting results in (L) ($n = 3$). (N) Luciferase assay comparing the amplification of NF- κ B activity by 4-1BB WT and 4KR. Plasmids were transfected to the HEK293T/NF- κ B reporter cell line and harvested to analyze the NF- κ B reporter activity by measuring bioluminescence ($n = 4$). The values are presented as mean \pm SD. N.S. $P > 0.05$; * $P < 0.05$, ** $P < 0.01$ (two-tailed student's t -test). MFI, mean fluorescence intensity. RLU, relative luminescence unit.

mutant of 4-1BB in parallel. EGFP was fused downstream of 4-1BB with a T2A self-cleavage peptide to monitor the lentivirus transduction. As displayed in Fig. 3D–E, the 4-1BB 4KR mutant exhibited substantially elevated membrane level as against WT, supporting the delayed turnover and increased accumulation of 4KR than WT. Taken together, these results cooperatively confirmed that 4-1BB degradation is dictated by ubiquitination on its 4-K motif. UPS-mediated degradation is the most fundamental mechanism guiding the clearance of target proteins; therefore, we sought to investigate whether ubiquitination functions as a signal to transport 4-1BB to the proteasomal degradation pathway. Upon the treatment of proteasome inhibitor MG-132, the protein level of 4-1BB could be rapidly upregulated in lymphoid (Hodgkin's lymphoma cell line HDLM-2) and epithelial cells (non-small cell lung cancer cell line H1975) in 6 h without increases of mRNA level (Fig. 3F–I), suggesting that 4-1BB is degraded through UPS mechanism. A similar effect can be phenotypically reproduced on exogenously expressed 4-1BB in both Jurkat and HEK293T cells (Fig. 3J–K), indicating the effect of MG-132 was achieved by posttranslational mechanisms. As anticipated, degradation of 4-1BB was retarded with proteasome inhibition by MG-132 (Fig. 3L–M). Since polyubiquitin chains can be utilized by some proteins as signal transduction scaffolds, we compared the potential of 4-1BB WT and 4KR to drive the activation of NF- κ B which is known to be the major transcription factor that 4-BB signals through. Unsurprisingly, transient transfection of 4-1BB 4KR elicited stronger NF- κ B activity in comparison to WT (Fig. 3N), suggesting that the polyubiquitin chain is unlikely to contribute to 4-1BB signaling, and the delayed degradation of 4-1BB may lead to augmented transcription of downstream genes. These data collectively confirm that the abundance and biological functions of 4-1BB are negatively regulated by the UPS-mediated proteolysis.

Ubiquitination-mediated proteolysis of 4-1BB depends on its *N*-glycosylation status

We then evaluated the expression pattern of 4-1BB WT and 4KR from whole cell lysate by immunoblotting. It met our expectation that 4KR had increased band intensity than WT due to its slow turnover; however, the different bands of 4-1BB showed unidentical ratio change. As demonstrated in Fig. 4A, the higher membrane expression of the 4-1BB 4KR mutant (Fig. 3D,E) is associated only with the increased high molecular weight (high-MW) band on immunoblotting, giving rise

to the hypothesis that high-MW band of 4-1BB confers the mature, membrane-localized form, and is more sensitive to UPS-mediated degradation. 4-1BB is a heavily glycosylated protein with two putative *N*-glycosylation sites (N138 and N149 for humans, as shown in Fig. 4B) on the basis of the consensus motif (N-X-S/T) [34]. Asparagine-to-glutamine mutation of these two residues abolished the *N*-glycosylation and resulted in a band shift toward lower molecular weight. In agreement with that, digestion of 4-1BB by PNGase F, an enzyme that selectively cleaves N-linked glycans from the substrates, led to the vanishing of both high- and medium-MW bands of wild type 4-1BB in Jurkat cells (Fig. 4C), indicating that high- and medium-MW bands represent 4-1BB at distinct *N*-glycoforms. There are no additional N-linked glycosylation sites since 4-1BB N138Q/N149Q (2NQ) showed no response to PNGase F. Pharmacologically hindering protein transportation from the endoplasmic reticulum (ER) to Golgi apparatus by brefeldin A (BFA) treatment causes the decrease of only high-MW bands and accumulation of medium-MW bands in a time-dependent manner (Fig. 4D), indicating that the two bands represent distinct forms 4-1BB at pre- and post-Golgi compartments. Interestingly, short-time BFA treatment led to a significant decrease of high-MW 4-1BB WT rather than 4KR, which is consistent with our previous hypothesis that high-MW 4-1BB is sensitive to ubiquitination-triggered clearance. Considering protein *N*-glycosylation is achieved by sequential enzymatic reactions taking place in ER and Golgi, we presumed that medium MW is referred to as partially *N*-glycosylated 4-1BB which is generated in the ER, whereas the high-MW band is the mature 4-1BB that has passed the entire *N*-glycosylation pathway. To test the assumption that the high-MW band represents the membrane-localized 4-1BB, we exploited the cell membrane proteome labeling method with cell-impermeable sulfo-NHS-SS-biotin as demonstrated in Fig. 4E. We found that the biotinylated 4-1BB enriched by streptavidin pull-down was constituted mainly by the high-MW form over the other species. Altogether, we proposed that the high-MW bands represent 4-1BB at the fully *N*-glycosylated status, while the medium-MW ones stood for the ER-resident, partially *N*-glycosylated form. The rapid degradation of mature 4-1BB, which underwent the entire *N*-glycosylation process, was mediated by the polyubiquitination on the intracellular domain.

Profiling the interacting partners of 4-1BB

Protein degradation involves the sophisticated cellular machinery composed by a group of interacting partners. E3 ligase is known as the key component to

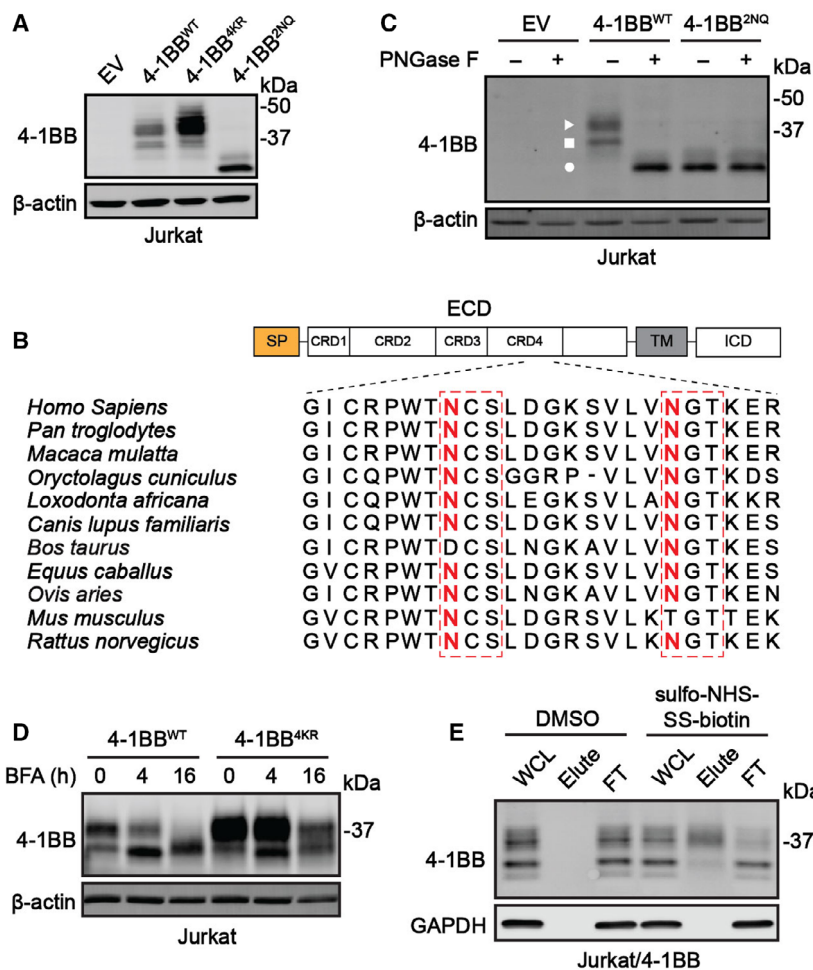


Fig. 4. Highly glycosylated 4-1BB is more susceptible to ubiquitination-mediated degradation. (A) Immunoblotting analysis of 4-1BB WT, 4KR, and 2NQ from Jurkat cells transduced with indicating lentivirus. (B) Immunoblotting analysis of PNGase F digestion of lysate from Jurkat cells stably expressing 4-1BB WT and 2NQ mutant. The 4-1BB mutants were lentivirally expressed on Jurkat cells. (C) Amino acid sequence alignment of mammalian 4-1BB on its *N*-glycosylation region at the extracellular domain. (D) Impact of BFA treatment to 4-1BB WT and 4KR by immunoblotting. Jurkat cells were transduced with lentivirus encoding 4-1BB WT or 4KR, then incubated with 1 μ M BFA for the indicated times. (E) Enrichment of membrane-associated 4-1BB by the sulfo-NHS-SS-biotin labeling strategy. The membrane proteome of Jurkat/4-1BB cells was labeled, enriched, and analyzed by immunoblotting. Triangle, high-MW band (mature form) of 4-1BB. Square, medium-MW band (immature form) of 4-1BB. Circle, low-MW band (*N*-glycan-abolished form) of 4-1BB. FT, flow-through.

promote target ubiquitination and allow proteolysis to take place predominantly but not exclusively through the proteasomal pathway. Therefore, we planned to carry out proteomics-based approaches to comprehensively profile the intracellular binding partners of 4-1BB. Considering the transient nature of E3 ligase-substrate interaction, which made it challenging to capture E3 ligases by affinity pulldown, we alternatively conducted the BioID assay which is an ideal approach to map the weak or transient interacting partners of a given protein of interest (“bait”; Fig. 5A) [35]. Besides, several reports have shown that proximity labeling can be utilized to identify E3 ligases/deubiquitinating enzymes of given substrates [36], which further justified the feasibility of our research strategy. To set up the BioID assay, BioID2 (an optimized promiscuous biotin ligase with smaller size and superior labeling efficiency [36]) was fused to the cytoplasmic end of human 4-1BB with a hemagglutinin (HA) tag (4-1BB-BioID2-HA) and was stably expressed in the HEK293FT cell line. The labeling efficiency of

proximal proteins was validated by streptavidin blotting before the mass spectrometry sample collection (Fig. 5B). Cells expressing the BioID2-HA construct were utilized to exclude the proteins that were randomly labeled in cells. We applied stringent data filtration criteria, and only proteins with unique peptides recognized in all three biological replicates were considered meaningful hits. As expected, 4-1BB was significantly enriched in the 4-1BB-BioID2 group with a fold change (FC) > 8 according to label-free quantification (LFQ; Fig. 5C), indicating that the labeling process was performed successfully. Consequently, a total of 362 enriched in 4-1BB-BioID2 group, of which 264 hits were considered significant (FC > 2, $P < 0.01$).

FBXL20 acts as the E3 ligase promoting 4-1BB ubiquitination and degradation

We next searched for E3 Ub ligase from the 264 candidates against a list of human E3 ligase assembled by

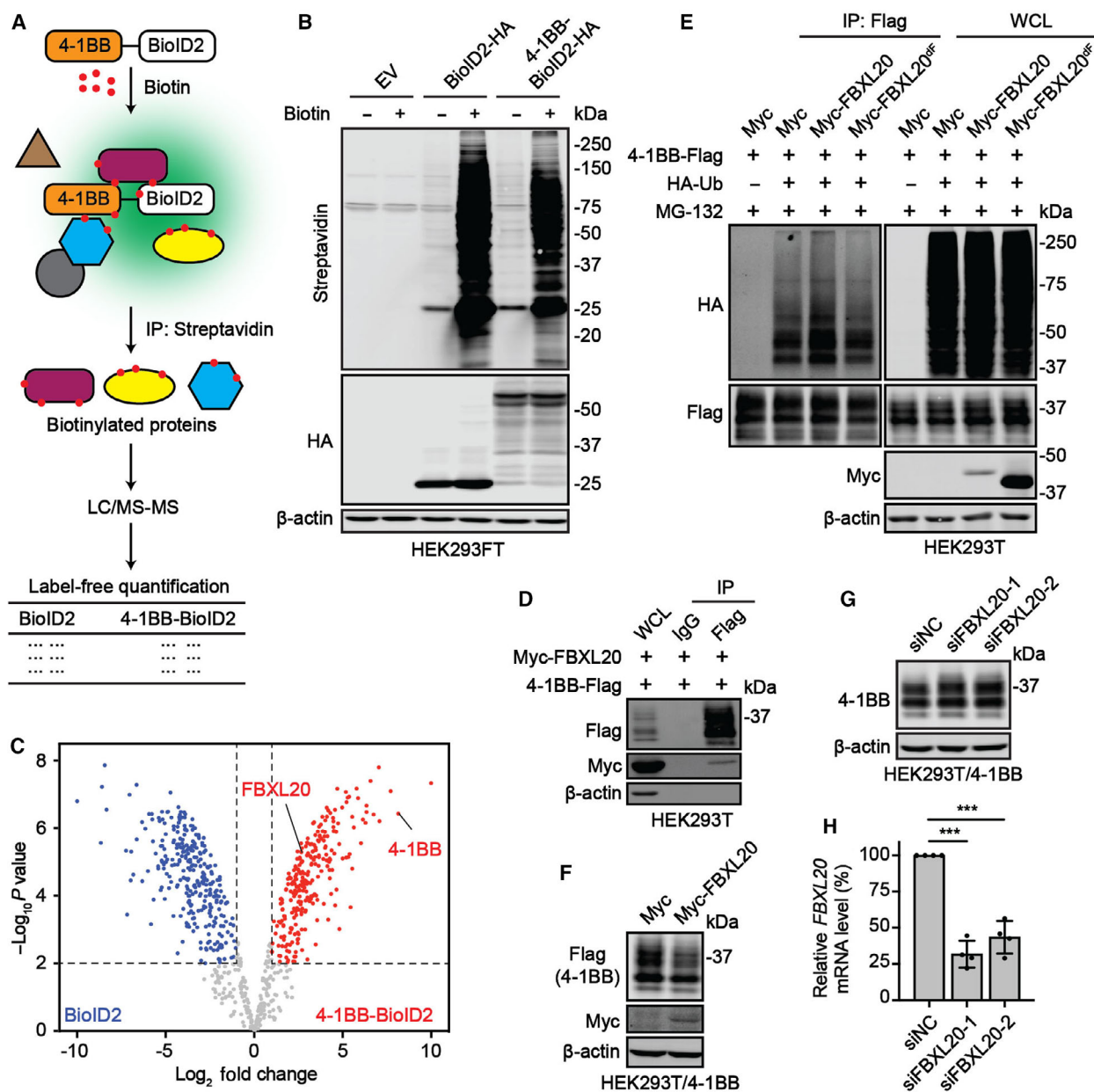


Fig. 5. FBXL20 promotes the polyubiquitination and degradation of 4-1BB. (A) Graphic workflow of BioID-based proximity labeling assay. (B) Validation of target biotinylation in BioID cell lines by streptavidin blotting. Lysates of biotin-treated cells were subjected to immunoblotting and visualized with IRDye800-conjugated streptavidin. (C) Volcano plot illustrating the differentially enriched biotinylated proteins in the BioID2 group versus the 4-1BB-BioID2 group. Three replicated sets of samples were included for LFQ. Significant hits ($FC > 2$, $P < 0.01$) were highlighted (BioID2 group by blue dots, and 4-1BB-BioID2 group by red dots). (D) Co-IP confirmation of 4-1BB-FBXL20 interaction. HEK293T cells were cotransfected with 4-1BB-Flag and Myc-FBXL20 plasmids followed by anti-Flag immunoprecipitation. (E) Assessment of FBXL20-promoted polyubiquitination of 4-1BB. Myc-FBXL20 and HA-Ub plasmids were cotransfected to the HEK293T/4-1BB cell line followed by *in vivo* ubiquitination assay. (F) Immunoblotting results of 4-1BB protein level change on the HEK293T/4-1BB cell line upon transfection of the empty vector or Myc-FBXL20 plasmid. (G) Immunoblotting showing 4-1BB protein level change on HEK293T/4-1BB cell line upon the transfection of non-targeting or FBXL20-targeting siRNA. (H) Validation of FBXL20 knockdown by measuring the mRNA level through qPCR ($n = 4$). The values are presented as mean \pm SD. *** $P < 0.001$ (two-tailed Student's *t*-test). LC-MS/MS, liquid chromatography-tandem mass spectrometry. EV, empty vector. siNC, non-targeting siRNA.

Tokheim et al. [37]. Notably, FBXL20 was the only E3 ligase that could be identified from all three replicates of 4-1BB- BioID2 samples but not the BioID2 samples (Fig. 5C), suggesting FBXL20 serves as a 4-1BB interacting protein with high reliability. FBXL20, also known as SCRAPPER, was originally identified from the central nervous system [38]. Sequence analysis confirmed SCRAPPER as a member of the F-box family E3 ligase according to its F-box domain on N-terminus. F-box proteins function as the substrate recognition subunit and cooperate with S phase kinase-associated protein 1 (SKP1) and cullin 1 (CUL1) to form SCF complexes that have intact E3 ligase activity [39]. The SCF E3 ligase complex mediates the degradation of a wide range of proteins. Among over 70 members of F-box family proteins, the substrate specificity and biological importance of FBXL20 are less clarified. Our preliminary results from BioID screening prompted us to interrogate whether 4-1BB expression is regulated through FBXL20-mediated polyubiquitination. The interaction of 4-1BB and FBXL20 was confirmed by coimmunoprecipitation (co-IP) assay as demonstrated in Fig. 5D. As expected, overexpression of FBXL20 led to an increased polyubiquitination level of 4-1BB. However, the F-box-deleted mutant of FBXL20 (FBXL20^{ΔF}), which cannot complex with SKP1 and CUL1 to form SCF complex, failed to ubiquitinate 4-1BB (Fig. 5E). Overexpression of FBXL20 led to a decrease of 4-1BB (Fig. 5F). Conversely, siRNA-mediated FBXL20 knockdown resulted in the accumulation of total 4-1BB (Fig. 5G,H). We then took advantage of bioinformatics platforms to study the impact of FBXL20 on cancer immunotherapy. As unveiled by TCGA datasets, FBXL20 expression was inversely correlated with the overall survival of individuals harboring kidney renal papillary cell carcinoma (KIRP) and ovarian serous cystadenocarcinoma (OV;

Fig. 6A,B). More importantly, high FBXL20 expression is associated with less satisfactory clinical outcome of checkpoint therapy in two independent cohorts (Fig. 6C,D) as unveiled by the TIDE database. These data suggested that FBXL20 may serve critical roles in antitumor immunity, and this is possibly related to its regulatory function on 4-1BB.

Discussion

In this study, we reported that the E3 ligase subunit FBXL20 drives the proteasomal degradation of 4-1BB by prompting the polyubiquitination on the four intracellular lysine residues. The physiological essentiality of 4-1BB as an immune stimulator has been well-documented. For instance, systematic deletion of 4-1BB showed diminished T cell immunity in mice [40]. Clinically, several loss-of-function mutations of 4-1BB have been reported to be correlated with defected T cell and B cell immunity and enhance the susceptibility to Epstein–Barr virus (EBV)-associated lymphoma [41]. The DNA hypomethylation on *TNFRSF9* loci, which led to increased transcription of 4-1BB, is positively correlated with antitumor immunity and survival in melanoma patients [42]. Nonetheless, the unexpected activation of 4-1BB signaling on non-T cells was found to accelerate pathogenesis or induce severe adverse effects upon the systematic administration of therapeutic antibodies. As indicated by Bartkowiak et al., activation of liver-resident myeloid cells via 4-1BB pathway triggers IL-27-dependent liver damage [43]. Jiang et al. showed that 4-1BB promotes the differentiation of monocytes/macrophages and facilitates the bone metastasis of breast cancer [44]. 4-1BB⁺ B cells secrete proinflammatory cytokines such as TNF α and IL-6 upon engagement with 4-1BBL-expressing cells and led to multiple sclerosis [45]. The

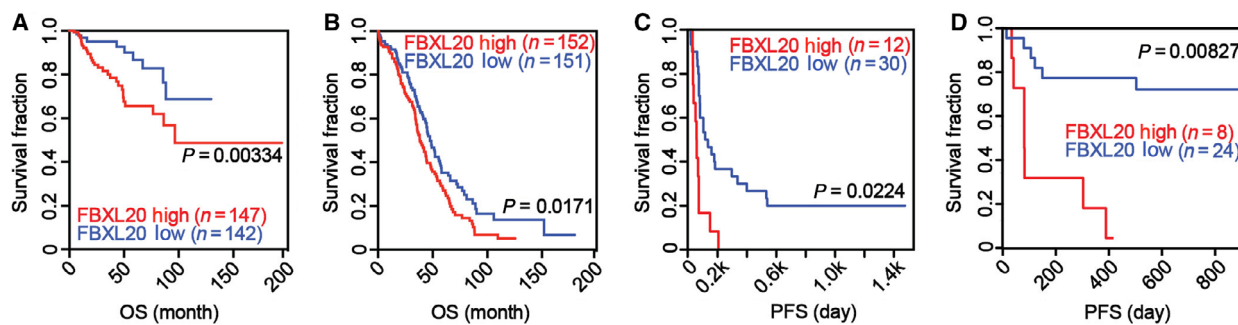


Fig. 6. Impact of FBXL20 in cancer development and therapeutical outcome. (A–B) Inverse correlation of *FBXL20* mRNA level with the overall survival from TCGA-KIRP (A) and TCGA-OV (B) datasets. (C–D) Inverse correlation of the *FBXL20* mRNA level and immunotherapy outcomes in two cohorts of melanoma patients (C, dataset phs000452.v2.p1, $n = 42$; D, dataset PRJEB23709, $n = 32$). Significance values were calculated by log-rank analysis.

upregulation of 4-1BB can also be found on adipocytes upon obesity-related factors and promotes adipose inflammation [46]. Conversely, deficiency of 4-1BB protects mice against obesity-induced inflammation [47]. 4-1BB is involved in cardiovascular diseases as well. According to a study by Olofsson et al. [48], the expression of 4-1BB on vascular endothelial cells and contributes to the development of atherosclerosis. In summary, the biological behaviors and functions of 4-1BB are rather complicated and likely to be tissue- and cell lineage-dependent, and the profound understanding of their differentiated regulation would help resolve the dilemma of how to precisely target 4-1BB on tumor-reactive T cells.

The presence of the target is the basis of efficacious drug therapy; therefore, it is of great significance to investigate the regulatory mechanisms controlling the abundance of proteins that serve as drug targets. As the first broadly applied immunotherapeutic targets, PD-1 undergoes ubiquitination for degradation, and different E3 ligases favor PD-1 at distinct glycosylation status. While FBXO38 was identified by Meng et al. as the E3 ligase destabilizing mature PD-1 inserted on T cell membrane [49], KLHL22 ubiquitinates the partially glycosylated PD-1 before it reaches Golgi apparatus [50]. The functional participation of ubiquitination in regards of the 4-1BB signaling pathway has been discussed in a few studies. Forero et al. unveiled that K63-linked ubiquitination of the adapter protein TRAF2 is required for the downstream signal activation upon antibody-mediated 4-1BB stimulation [9]. By contrast, deubiquitinase A20 and CYLD are both associated with 4-1BB/TRAF2 signal complex and dampen the NF- κ B activation by disassembling the polyubiquitin chain on TRAF2 [51]. These studies provided valuable insights linking 4-1BB signaling with protein ubiquitination. In our research, we demonstrated that FBXL20-promoted ubiquitination is involved in the modulation of 4-1BB by directing its proteolysis. According to Guo et al. [52], GITR can also be proteasomally degraded, suggesting potential degradation mechanisms shared by TNFRSF family immune receptors. Another highlighted finding in our study is that we noticed the unidentical pattern of proteasomal degradation of 4-1BB at distinct glycoforms. The interplay between glycosylation and ubiquitination has been reported on many proteins. Previous studies reported that *N*-glycosylation of immune receptors can directly or indirectly impede E3 ligase engagement and, therefore, enhance their stability [53,54]. Conversely, some E3 ligase functions by specifically recognizing *N*-glycosylated degron on substrates [55]. We hypothesized that *N*-glycosylation affects 4-1BB stability possibly through regulating its spatial distribution instead of E3

ligase recruitment for two reasons: first, the post-Golgi fraction of 4-1BB is more sensitive to UPS-mediated degradation than the pre-Golgi fraction. It has been reported that FBXL20 contains a C-terminal isoprenylated CAAX membrane sorting signal [56], which allows it to engage the surface 4-1BB and promote degradation; second, the intracellular domain (ICD) and the extracellular *N*-glycosylation motifs of 4-1BB are separated into distinct subcellular compartments by the plasma membrane. Given that the ubiquitination of 4-1BB occurs on the ICD, it is very likely that FBXL20 recognizes the ICD-localized degron regardless of the *N*-glycosylation status on the extracellular domain. Nevertheless, the crosstalk between these two modifications on 4-1BB should be further explored in depth.

One limitation of our study is that we have not delineated how FBXL20 recognizes 4-1BB. As reviewed, F-box proteins are recruited to substrates by a variety of means [57]. In the research by Xiao et al., FBXL20 drives ubiquitination-dependent degradation of Vsp34, and key degron of Vsp34 was identified to be the phosphorylated T159 residue [56]. Recently, Manne et al. described that proapoptotic proteins PUMA and BAX are both degraded by FBXL20-induced K48-linked polyubiquitination, and this process is licensed by Akt-mediated phosphorylation of substrates [58]. Notably, the degradation rate of 4-1BB was only partially rescued by MG-132, whereas the 4KR mutant remained at high intracellular abundance after CHX treatment for 12 h. According to our preliminary observation, the lysosomal-autophagy pathway is also involved in the control of 4-1BB abundance (data not shown), suggesting additional mechanisms by which the ubiquitination signal on the ICD is utilized to guide 4-1BB degradation.

In conclusion, we revealed that 4-1BB is a ubiquitinated protein that undergoes UPS-mediated rapid degradation. Proteomics analysis identified FBXL20 serves as one of the E3 ligases to ubiquitinate and destabilize 4-1BB. Data mining results also indicated that FBXL20 is negatively correlated with the clinical benefits gained from checkpoint inhibitors, supporting the potential of FBXL20 to act as a key predictor of immunotherapy for cancer. Our research also provided a practical paradigm to interrogate the molecular nature of other TNFRSF family proteins.

Materials and methods

Cell culture

HEK293FT, Jurkat, H1975, and B16F10 cells were obtained from American Type Culture Collection

(Manassas, VA, USA). HEK293T cells were purchased from Takara (San Jose, CA, USA). HDLM-2 cells were purchased from Creative Bioarray (Shirley, NY, USA). Jurkat cells were cultured in RPMI-1640 medium (Cytiva, Marlborough, MA, USA) containing 10% FBS (Corning, Oneonta, NY, USA), 2 mM L-glutamine, 10 mM HEPES, 1 mM sodium pyruvate, and 1% penicillin/streptomycin (Pen/Strep; Gibco, Waltham, MA, USA). HDLM-2 cells were cultured in RPMI medium with 20% FBS and antibiotics. All other cell lines were maintained in Dulbecco's Modified Eagle Medium (Gibco) with 10% FBS and pen/strep. All cells were kept in humidified incubators with 5% CO₂ at 37 °C.

Plasmid transfection and RNA interference

The cDNA of human (Sino Biological, Wayne, PA, USA) and mouse (Genescript, Piscataway, NJ, USA) 4-1BB were cloned into the pcDNA3 vector for transient transfection. For lentivirus-mediated protein expression, human 4-1BB was cloned into pCDH-CMV-puro (System Biosciences, Palo Alto, CA, USA) and pHR-SFFV (Addgene, Watertown, MA, USA, #79121) vector for stable expression. The cDNA of human FBXL20 (DNASU, Tempe, AZ, USA, #HsCD00942792) was cloned to the pcDNA3 vector. Point mutations were accomplished by using the Q5 Site-Directed Mutagenesis Kit (New England BioLabs, Ipswich, MA, USA). The construction of other plasmids was described in the corresponding sections in detail. All DNA constructs were confirmed by Sanger sequencing before use. Knockdown of FBXL20 was achieved by siRNA transfection. The siRNA targeting human FBXL20 was purchased from Integrated DNA Technologies (Coralville, IA, USA). Transfections of DNA and siRNA were performed using X-TremeGene HP (Roche, Indianapolis, IN, USA) and Lipofectamine RNAiMAX transfection reagent (Invitrogen, Waltham, MA, USA), respectively, according to the manufacturer's guidance.

Stable cell line generation by lentivirus

Lentiviral plasmids of target genes were cotransfected with pMD2.G (Addgene #12259) and psPAX2 (Addgene #12260) to HEK293T cells at a 4 : 2 : 3 ratio. Forty-eight hours after transfection, the supernatant was collected and utilized for transduction of target cells. For transduction of Jurkat cells, lentivirus was incubated with cells overnight, and protein expression was confirmed on day 3 by flow cytometry or Western blotting. To transduce adherent cell lines, the lentivirus-containing supernatant was added to cell culture in the presence of 8 µg·mL⁻¹ polybrene (Santa Cruz Biotechnology, Dallas, TX, USA) overnight. Stable cell lines were acquired by puromycin selection.

Immunoblotting, immunoprecipitation, and *in vivo* ubiquitination assay

For immunoblotting, cells were lysed in RIPA lysis buffer (50 mM Tris-HCl, pH 7.5, 150 mM NaCl, 1% NP-40, 0.1% SDS, 1 mM EDTA, 0.5% sodium deoxycholate, 1 µg·mL⁻¹ pepstatin, 2 µg·mL⁻¹ aprotinin, 2 µg·mL⁻¹ leupeptin and 1 mM PMSF), centrifuged at 20 000 *g* for 15 min, and boiled in laemmli buffer containing 5% 2-mercaptoethanol (2-ME) for 10 min at 95 °C. The concentration of samples was determined by BCA assay (Pierce, Waltham, MA, USA). Samples were separated on SDS/PAGE gels and transferred onto PVDF membranes (Millipore, St. Louis, MO, USA) followed by blocking in 5% skim milk. Membranes were sequentially incubated with primary antibodies at 4 °C overnight and secondary antibodies (LI-COR Biosciences, Lincoln, NE, USA) at room temperature for 1 h. Image acquisition was performed on Odyssey CLx imager (LI-COR Biosciences). Band intensity quantification was completed on Image Studio software. For immunoprecipitation, cells were lysed in ice-cold NETN lysis buffer (50 mM Tris-HCl, pH 7.5, 150 mM, 0.5% NP-40, 1 mM EDTA, 1 µg·mL⁻¹ pepstatin, 2 µg·mL⁻¹ aprotinin, 2 µg·mL⁻¹ leupeptin and 1 mM PMSF) on a shaker for 30 min. Lysates were clarified by centrifugation (20 000 *g*, 15 min, 4 °C) and incubated with antibody-conjugated agarose beads overnight followed by four times washing. Bead-bound proteins were eluted by boiling in sample buffer containing 2-ME for 10 min at 95 °C. Samples were analyzed by immunoblotting. To detect protein ubiquitination, cells were incubated with 20 µM MG-132 (Selleck, Houston, TX, USA) for 4 h and lysed in NETN buffer. Clarified cell lysates were supplemented with 1% SDS and incubated at 95 °C for 10 min to dissociate the non-specifically bound proteins. Afterward, nine volumes of SDS-free NETN buffer were added to the lysate afterward to dilute SDS concentration to 0.1% for immunoprecipitation overnight. The following steps for sample analysis were performed the same as immunoprecipitation above. The following primary antibodies and beads were used for detection: anti-Flag agarose (Sigma Aldrich, St. Louis, MO, USA, #A2220), Flag-tag (Sigma Aldrich #F1804, 1 : 1000, mouse), DYKDDDDK-tag (Cell signaling technology, Danvers, MA, USA, #2368, 1 : 2000, rabbit, same as Flag-tag), β-actin (Santa Cruz #sc-47778, 1 : 1500, mouse), GAPDH (Cell signaling technology #5174, 1 : 2500, rabbit), HA-tag (Cell signaling technology #3724, 1 : 2500, rabbit), Myc-tag (Cell signaling technology #2278, 1 : 1000, rabbit), and 4-1BB (Cell signaling technology #34594, 1 : 2500, rabbit).

RNA isolation and qRT-PCR

Total RNA was extracted from cells by using TRIzol reagent (Invitrogen). 1 µg total cellular RNA was used for cDNA synthesis with the iScript cDNA Synthesis Kit (Bio-Rad, Hercules, CA, USA) according to the guidance by the

manufacturer. Real-time PCR was performed using SsoAdvanced Universal SYBR Green Supermix (Bio-Rad) on a CFX96 real-time PCR system (Bio-Rad). The relative gene expression was normalized to β -actin and calculated by the $\Delta\Delta C_q$ method. The following primers were used for qRT-PCR amplification:

Human β -actin forward: 5'- AGAGCTACGAGCTGCC TGAC -3'

Human β -actin reverse: 5'- AGGAAGGAAGGCTGGAA GAG -3'

Human 4-1BB forward: 5'- CGCTCCGTTTCTCTGTTG TTA -3'

Human 4-1BB reverse: 5'- GCTACAGCCATCTTCCTC TTG -3'

Human FBXL20 forward: 5'- TAGCCAGGTGAAGCA TTGAG -3'

Human FBXL20 reverse: 5'- AGAGGGTGCTTCTTC TTGGA -3'

NF- κ B reporter assay

The NF- κ B reporter cell line was generated by transducing HEK293T cells with pGreenfire-NF- κ B-puro lentivirus (System Biosciences). Cells were transfected with 4-1BB plasmids and harvested in passive lysis buffer (Promega, Madison, WI, USA) 48 h after transfection. The reporter activity was measured using Bio-Glo luciferase substrate (Promega) on a Synergy LX plate reader (BioTek, Winowski, VT, USA) and normalized to protein concentration.

Mass spectrometry

For detection of ubiquitination signal, 4-1BB with a C-terminus Flag tag was isolated using anti-Flag M2 affinity gel (Sigma Aldrich #A2220) from HEK293T/4-1BB cells. To increase the abundance of ubiquitinated protein, cells were pre-treated with 20 μ M MG-132 for 4 h before protein extraction. Bound proteins were eluted by 3 \times Flag peptide (Sigma Aldridge), resolved by SDS/PAGE gel and visualized by Coomassie blue staining. The gels were minced and rinsed with 50% acetonitrile/20 mM ammonium bicarbonate (pH 7.5) twice. The gel pieces were dehydrated with acetonitrile and dried out on SpeedVac. Protein was on-gel digested by 0.01 mg·mL⁻¹ trypsin in 20 mM NH₄HCO₃. The tryptic peptides were extracted from gel pieces with 50% acetonitrile/0.1% formic acid twice and dried. The mass spectrometry analyses were performed on a LTQ Orbitrap Elite Mass Spectrometer coupled with a Proxeon Easy NanoLC system (Thermo Scientific, Waltham, MA, USA). The data-dependent acquisition (DDA) method was used to acquire MS data. A survey MS scan was acquired first, and then the top eight ions in the MS scan were selected for following CID MS/MS analysis. Both MS and MS/MS scans were acquired by Orbitrap at the resolutions of 120 000 and 15 000, respectively. Data were acquired using Xcalibur software (version 2.2; Thermo Fisher

Scientific). Protein identification and modification characterization were performed using Thermo Proteome Discoverer (version 1.4) with the Mascot (Matrix Science) and Uniprot human protein databases (protein count: 78 120, Proteome ID: UP000005640). The spectra of possible modified peptides were further inspected to verify the accuracy of the assignments.

To employ BioID assay, we first established HEK293FT cell lines stably expressing the BioID constructs. HA-tagged BioID2 was subcloned from MCS-BioID2-HA (Addgene #74224) to the pGIPZ vector to get control plasmids (pGIPZ_BioID2-HA). The pGIPZ_h4-1BB-BioID2-HA construct was acquired by inserting human 4-1BB cDNA upstream of BioID2 with a GGGGS linker. Lentivirus transduction and puromycin selection were described previously. Cells were pre-treated with 50 μ M D-biotin (Alfa Aesar, Tewksbury, MA, USA) for 24 h to biotinylate the proximal proteome of 4-1BB. After three washes with ice-cold PBS buffer, cells were pelleted and stored at -80 °C for protein enrichment later. Three biological replicated sets of samples were prepared independently. The isolation of biotinylated protein was conducted as described [36]. In short, biotinylated protein was precipitated by high-capacity streptavidin agarose (Pierce). 5% of agarose was used for validating the protein biotinylation, and the rest of the protein-bound beads were suspended in 50 mM NH₄HCO₃ and stored at -80 °C before LC/MS-MS analysis. Three biological replicates of samples were prepared independently. The raw data were processed by MaxQuant (v2.0.3.0) and searched against the UniProt human protein database. The false discovery rate was set to 0.01. Fold change along with *P* values of all identified proteins were analyzed and visualized using the LFQ-Analyst platform (<https://bioinformatics.erc.monash.edu/apps/LFQ-Analyst/>) [59]. The proteomic analysis was performed on the Thermo Orbitrap Elite LC/MS system (funded by NIH S10RR028859) at the Proteomics and Mass Spectrometry Facility at University of Georgia.

Flow cytometry

The membrane level of 4-BB was evaluated by flow cytometry. Lentivirus-transduced Jurkat cells were washed twice with washing buffer (0.5% BSA in PBS) and incubated with APC-conjugated human 4-1BB antibody (BD #561702) for 30 min at 4 °C. Antibody-stained cells were loaded on Attune NxT Flow Cytometer (Invitrogen) for analysis. EGFP⁺ population of cells was gated to determine the membrane level of 4-1BB. To acquire convincing quantitative result, lentivirus-transduced cells must have a comparable overall EGFP signal to be used for MFI measurement. The data were visualized and analyzed on Attune NXT software (Invitrogen).

Membrane protein labeling

To label membrane-bound proteins, cells were washed twice with ice-cold PBS. Cells were incubated with 1 mg·mL⁻¹

sulfo-NHS-SS-biotin (APEX-BIO, Houston, TX, USA) for 30 min at 4 °C. The biotinylation reaction was quenched by 100 mM glycine in PBS, and total protein was extracted in RIPA buffer. The biotinylated protein was isolated with high-capacity streptavidin agarose (Pierce) overnight at 4 °C and eluted by sample buffer with 2-ME. All samples were analyzed by immunoblotting.

PNGase F assay

The N-linked glycosylation of 4-1BB is analyzed by glycosidase treatment. 4-1BB-expressing cells were lysed in NETN buffer and subjected to Rapid PNGase F (New England BioLabs) following the protocol provided by the manufacturer. The enzymatic digestion results were analyzed by immunoblotting as described above.

Statistical analysis

Quantification was performed using GRAPHPAD PRISM 9 (GraphPad Software, San Diego, CA, USA) or Microsoft Excel (Microsoft, Redmond, WA, USA). Two-tailed student's *t*-test was used to calculate the significance between the two groups. A *P* value < 0.05 was considered statistically significant. All quantitative experimental results were presented as mean ± SD, calculated from at least three replicates. The infiltration level of immune cells was assessed by TIMER or CIBERSORT and visualized on TIMER2.0 (<http://timer.cistrome.org/>). The impact of genes on overall survival was analyzed based on TCGA dataset on cBioPortal (<https://www.cbioportal.org/>). TIDE (<http://tide.dfci.harvard.edu/>) was exploited for evaluating the correlation between genes and immunotherapy outcome.

Acknowledgements

This study was funded in part by Susan G. Komen Breast Cancer Foundation (CCR17488088); Ralph W. and Grace M. Showalter Research Trust grant; Purdue Institute for Drug Discovery (PIDD) Programmatic Area grant; Purdue Center for Cancer Research. The authors acknowledge the use of the Chemical Genomics Facility, a core facility of Purdue Institute for Drug Discovery and the NIH-funded Indiana Clinical and Translational Sciences Institute.

Conflict of interest

The authors declare no conflict of interest.

Author contributions

Experiments and data analysis were completed by RS. SOL designed and supervised the study. RS and SOL prepared the manuscript together.

Peer review

The peer review history for this article is available at <https://publons.com/publon/10.1111/febs.16383>.

Data availability statement

All data presented in this article is available upon request.

References

- 1 Billan S, Kaidar-Person O, Gil Z. Treatment after progression in the era of immunotherapy. *Lancet Oncol.* 2020;**21**:e463–76.
- 2 Morad G, Helmink BA, Sharma P, Wargo JA. Hallmarks of response, resistance, and toxicity to immune checkpoint blockade. *Cell.* 2021;**184**:5309–37.
- 3 Mayes PA, Hance KW, Hoos A. The promise and challenges of immune agonist antibody development in cancer. *Nat Rev Drug Discov.* 2018;**17**:509–27.
- 4 Melero I, Johnston JV, Shufford WW, Mittler RS, Chen L. NK1.1 cells express 4-1BB (CDw137) costimulatory molecule and are required for tumor immunity elicited by anti-4-1BB monoclonal antibodies. *Cell Immunol.* 1998;**190**:167–72.
- 5 Kim JO, Kim HW, Baek KM, Kang CY. NF-kappaB and AP-1 regulate activation-dependent CD137 (4-1BB) expression in T cells. *FEBS Lett.* 2003;**541**:163–70.
- 6 Kucka K, Wajant H. Receptor oligomerization and its relevance for signaling by receptors of the tumor necrosis factor receptor superfamily. *Front Cell Dev Biol.* 2020;**8**:615141.
- 7 Zapata JM, Perez-Chacon G, Carr-Baena P, Martinez-Forero I, Azpilikueta A, Otano I, et al. CD137 (4-1BB) signalosome: complexity is a matter of TRAFs. *Front Immunol.* 2018;**9**:2618.
- 8 Melero I, Shuford WW, Newby SA, Aruffo A, Ledbetter JA, Hellstrom KE, et al. Monoclonal antibodies against the 4-1BB T-cell activation molecule eradicate established tumors. *Nat Med.* 1997;**3**:682–5.
- 9 Martinez-Forero I, Azpilikueta A, Bolanos-Mateo E, Nistal-Villan E, Palazon A, Teixeira A, et al. T cell costimulation with anti-CD137 monoclonal antibodies is mediated by K63-polyubiquitin-dependent signals from endosomes. *J Immunol.* 2013;**190**:6694–706.
- 10 Qi X, Li F, Wu Y, Cheng C, Han P, Wang J, et al. Optimization of 4-1BB antibody for cancer immunotherapy by balancing agonistic strength with FcγR2b affinity. *Nat Commun.* 2019;**10**:2141.
- 11 Chester C, Sanmamed MF, Wang J, Melero I. Immunotherapy targeting 4-1BB: mechanistic rationale, clinical results, and future strategies. *Blood.* 2018;**131**:49–57.

- 12 Tolcher AW, Sznol M, Hu-Lieskovan S, Papadopoulos KP, Patnaik A, Rasco DW, et al. Phase Ib study of utomilumab (PF-05082566), a 4-1BB/CD137 agonist, in combination with pembrolizumab (MK-3475) in patients with advanced solid tumors. *Clin Cancer Res.* 2017;**23**:5349–57.
- 13 Qi XY, Li FL, Wu Y, Cheng C, Han P, Wang JY, et al. Optimization of 4-1BB antibody for cancer immunotherapy by balancing agonistic strength with Fc gamma R affinity. *Nat Commun.* 2019;**10**:2141.
- 14 Fu SQ, Harb WA, Patel SP, Lu C, Halperin DM, Hsu YH, et al. Early safety and efficacy from a phase I open-label clinical trial of CD137(4-1BB) agonistic antibody LVGN6051 as monotherapy and in combination with pembrolizumab. *J Clin Oncol.* 2021;**39**:2521.
- 15 Ho SK, Xu ZH, Thakur A, Fox M, Tan SS, DiGiammarino E, et al. Epitope and Fc-mediated cross-linking, but not high affinity, are critical for antitumor activity of CD137 agonist antibody with reduced liver toxicity. *Mol Cancer Ther.* 2020;**19**:1040–51.
- 16 Compte M, Harwood SL, Munoz IG, Navarro R, Zonca M, Perez-Chacon G, et al. A tumor-targeted trimeric 4-1BB-agonistic antibody induces potent anti-tumor immunity without systemic toxicity. *Nat Commun.* 2018;**9**:4809.
- 17 Tolcher AW, Carvajal RD, El-Khoueiry AB, Feliu WO, Zang H, Ancukiewicz M, et al. Initial findings of the first-in-human phase I study of AGEN2373, a conditionally active CD137 agonist antibody, in patients (pts) with advanced solid tumors. *J Clin Oncol.* 2021;**39**.
- 18 Etxeberria I, Bolanos E, Teijeira A, Garasa S, Yanguas A, Azpilikueta A, et al. Antitumor efficacy and reduced toxicity using an anti-CD137 Probody therapeutic. *Proc Natl Acad Sci USA.* 2021;**118**:e2025930118.
- 19 Melero I, Geva R, Ben-Ami E, Maurice-Dror C, Calvo E, LoRusso P, et al. Phase I/IIa trial evaluating safety and clinical activity of DuoBody (R)-PD-L134-1BB (GEN1046) in advanced solid tumors. *Ann Oncol.* 2021;**32**:S313.
- 20 Hinner MJ, Aiba RSB, Jaquin TJ, Berger S, Durr MC, Schlosser C, et al. Tumor-localized costimulatory T-cell engagement by the 4-1BB/HER2 bispecific antibody-anticalin fusion PRS-343. *Clin Cancer Res.* 2019;**25**:5878–89.
- 21 Long AH, Haso WM, Shern JF, Wanhainen KM, Murgai M, Ingaramo M, et al. 4-1BB costimulation ameliorates T cell exhaustion induced by tonic signaling of chimeric antigen receptors. *Nat Med.* 2015;**21**:581–90.
- 22 Philipson BI, O'Connor RS, May MJ, June CH, Albelda SM, Milone MC. 4-1BB costimulation promotes CAR T cell survival through noncanonical NF-kappa B signaling. *Sci Signal.* 2020;**13**:eaay8248.
- 23 Dai Q, Han P, Qi XY, Li FL, Li M, Fan LL, et al. 4-1BB signaling boosts the anti-tumor activity of CD28-incorporated 2(nd) generation chimeric antigen receptor-modified T cells. *Front Immunol.* 2020;**11**:539654.
- 24 Woodsmith J, Kamburov A, Stelzl U. Dual coordination of post translational modifications in human protein networks. *PLoS Comput Biol.* 2013;**9**:e1002933.
- 25 Collins GA, Goldberg AL. The logic of the 26S proteasome. *Cell.* 2017;**169**:792–806.
- 26 Popovic D, Vucic D, Dikic I. Ubiquitination in disease pathogenesis and treatment. *Nat Med.* 2014;**20**:1242–53.
- 27 Sun SC. Deubiquitylation and regulation of the immune response. *Nat Rev Immunol.* 2008;**8**:501–11.
- 28 Hu H, Sun SC. Ubiquitin signaling in immune responses. *Cell Res.* 2016;**26**:457–83.
- 29 Malynn BA, Ma A. Ubiquitin makes its mark on immune regulation. *Immunity.* 2010;**33**:843–52.
- 30 Jiang P, Gu S, Pan D, Fu J, Sahu A, Hu X, et al. Signatures of T cell dysfunction and exclusion predict cancer immunotherapy response. *Nat Med.* 2018;**24**:1550–8.
- 31 Li T, Fan J, Wang B, Traugh N, Chen Q, Liu JS, et al. TIMER: A web server for comprehensive analysis of tumor-infiltrating immune cells. *Cancer Res.* 2017;**77**:e108–10.
- 32 Povlsen LK, Beli P, Wagner SA, Poulsen SL, Sylvestersen KB, Poulsen JW, et al. Systems-wide analysis of ubiquitylation dynamics reveals a key role for PAF15 ubiquitylation in DNA-damage bypass. *Nat Cell Biol.* 2012;**14**:1089–98.
- 33 Wagner SA, Beli P, Weinert BT, Nielsen ML, Cox J, Mann M, et al. A proteome-wide, quantitative survey of in vivo ubiquitylation sites reveals widespread regulatory roles. *Mol Cell Proteomics.* 2011;**10**:M111013284.
- 34 Helenius A, Aebi M. Intracellular functions of N-linked glycans. *Science.* 2001;**291**:2364–9.
- 35 Roux KJ, Kim DI, Burke B, May DG. BioID: a screen for protein-protein interactions. *Curr Protoc Protein Sci.* 2018;**91**:19 23 1–15.
- 36 Kim DI, Jensen SC, Noble KA, Kc B, Roux KH, Motamedchaboki K, et al. An improved smaller biotin ligase for BioID proximity labeling. *Mol Biol Cell.* 2016;**27**:1188–96.
- 37 Tokheim C, Wang X, Timms RT, Zhang B, Mena EL, Wang B, et al. Systematic characterization of mutations altering protein degradation in human cancers. *Mol Cell.* 2021;**81**:1292–1308.e11.
- 38 Yao I, Takagi H, Ageta H, Kahyo T, Sato S, Hatanaka K, et al. SCRAPER-dependent ubiquitination of active zone protein RIM1 regulates synaptic vesicle release. *Cell.* 2007;**130**:943–57.

- 39 Kipreos ET, Pagano M. The F-box protein family. *Genome Biol.* 2000;**1**:REVIEWS3002.
- 40 Kwon BS, Hurtado JC, Lee ZH, Kwack KB, Seo SK, Choi BK, et al. Immune responses in 4-1BB (CD137)-deficient mice. *J Immunol.* 2002;**168**:5483–90.
- 41 Somekh I, Thian M, Medgyesi D, Gülez N, Magg T, Gallón Duque A, et al. CD137 deficiency causes immune dysregulation with predisposition to lymphomagenesis. *Blood.* 2019;**134**:1510. –1516. <http://dx.doi.org/10.1182/blood.2019000644>
- 42 Fröhlich A, Loick S, Bawden EG, Fietz S, Dietrich J, Diekmann E, et al. Comprehensive analysis of tumor necrosis factor receptor TNFRSF9 (4-1BB) DNA methylation with regard to molecular and clinicopathological features, immune infiltrates, and response prediction to immunotherapy in melanoma. *EBioMedicine.* 2020;**52**:102647. <http://dx.doi.org/10.1016/j.ebiom.2020.102647>
- 43 Bartkowiak T, Jaiswal AR, Ager CR, Chin R, Chen CH, Budhani P, et al. Activation of 4-1BB on liver myeloid cells triggers hepatitis via an interleukin-27-dependent pathway. *Clin Cancer Res.* 2018;**24**:1138–51.
- 44 Jiang P, Gao W, Ma T, Wang R, Piao Y, Dong X, et al. CD137 promotes bone metastasis of breast cancer by enhancing the migration and osteoclast differentiation of monocytes/macrophages. *Theranostics.* 2019;**9**:2950–66.
- 45 Wong HY, Prasad A, Gan SU, Chua JJE, Schwarz H. Identification of CD137-expressing B cells in multiple sclerosis which secrete IL-6 upon engagement by CD137 ligand. *Front Immunol.* 2020;**11**:571964.
- 46 Tu TH, Kim CS, Goto T, Kawada T, Kim BS, Yu R. 4-1BB/4-1BBL interaction promotes obesity-induced adipose inflammation by triggering bidirectional inflammatory signaling in adipocytes/macrophages. *Mediators Inflamm.* 2012;**2012**:972629.
- 47 Kim CS, Kim JG, Lee BJ, Choi MS, Choi HS, Kawada T, et al. Deficiency for costimulatory receptor 4-1BB protects against obesity-induced inflammation and metabolic disorders. *Diabetes.* 2011;**60**:3159–68.
- 48 Olofsson PS, Soderstrom LA, Wagsater D, Sheikine Y, Ocaya P, Lang F, et al. CD137 is expressed in human atherosclerosis and promotes development of plaque inflammation in hypercholesterolemic mice. *Circulation.* 2008;**117**:1292–301.
- 49 Meng X, Liu X, Guo X, Jiang S, Chen T, Hu Z, et al. FBXO38 mediates PD-1 ubiquitination and regulates anti-tumour immunity of T cells. *Nature.* 2018;**564**:130–5.
- 50 Zhou XA, Zhou J, Zhao L, Yu G, Zhan J, Shi C, et al. KLHL22 maintains PD-1 homeostasis and prevents excessive T cell suppression. *Proc Natl Acad Sci USA.* 2020;**117**:28239–50.
- 51 Azpilikueta A, Bolanos E, Lang V, Labiano S, Aznar MA, Etxeberria I, et al. Deubiquitinases A20 and CYLD modulate costimulatory signaling via CD137 (4-1BB). *Oncoimmunology.* 2017;**7**:e1368605.
- 52 Guo Y, Yang L, Lei S, Tan W, Long J. NEDD4 negatively regulates GITR via ubiquitination in immune microenvironment of melanoma. *Onco Targets Ther.* 2019;**12**:10629–37.
- 53 Li CW, Lim SO, Xia W, Lee HH, Chan LC, Kuo CW, et al. Glycosylation and stabilization of programmed death ligand-1 suppresses T-cell activity. *Nat Commun.* 2016;**7**:12632.
- 54 Song X, Zhou Z, Li H, Xue Y, Lu X, Bahar I, et al. Pharmacologic suppression of B7-H4 glycosylation restores antitumor immunity in immune-cold breast cancers. *Cancer Discov.* 2020;**10**:1872–93.
- 55 Yoshida Y, Mizushima T, Tanaka K. Sugar-recognizing ubiquitin ligases: action mechanisms and physiology. *Front Physiol.* 2019;**10**:104.
- 56 Xiao J, Zhang T, Xu D, Wang H, Cai Y, Jin T, et al. FBXL20-mediated Vps34 ubiquitination as a p53 controlled checkpoint in regulating autophagy and receptor degradation. *Genes Dev.* 2015;**29**:184–96.
- 57 Skaar JR, Pagan JK, Pagano M. Mechanisms and function of substrate recruitment by F-box proteins. *Nat Rev Mol Cell Biol.* 2013;**14**:369–81.
- 58 Manne RK, Agrawal Y, Malonia SK, Banday S, Edachery S, Patel A, et al. FBXL20 promotes breast cancer malignancy by inhibiting apoptosis through degradation of PUMA and BAX. *J Biol Chem.* 2021;**297**:101253.
- 59 Shah AD, Goode RJA, Huang C, Powell DR, Schittenhelm RB. LFQ-analyst: an easy-to-use interactive web platform to analyze and visualize label-free proteomics data preprocessed with maxquant. *J Proteome Res.* 2020;**19**:204–11.